On the Stability of a Minimum-Loss Controlled Dual-VSI DFIG-DC System

Gil D. Marques
INESC - Id
Instituto Superior Técnico – Universidade de Lisboa
Lisbon, Portugal
gil.marques@tecnico.ulisboa.pt

Matteo F. Iacchetti
Department of Electrical and Computer Engineering
University of Manchester
Manchester, UK
matteo.iacchetti@manchester.ac.uk

Sérgio M. A. Cruz
Department of Electrical and Computer Engineering
University of Coimbra - IT
Coimbra, Portugal
smacruz@ieee.org

***Abstract*—Recently a minimum-loss control strategy for the Dual-VSI-DFIG system was proposed. It is implemented using three rules for the determination of the optimal stator frequency, of the stator/rotor magnetizing current split and of the airgap-flux magnitude. The method uses airgap-flux orientation with direct airgap flux and rotor current control. In this paper, two syntheses of the Proportional Integral controllers based respectively on the symmetrical optimum and on the ITAE criteria are presented. The stability is analyzed computing the eigenvalues of the closed loop model. For both cases the system is stable if the parameters are computed according to the synthesized rules. Instability can be found when these rules are not respected.**

Keywords—Control, DC power system, Dual-VSI DFIG, Efficiency improvement, Minimum loss control, Stability.

NOMENCLATURE

General

a	Design parameter of the symmetrical optimum criterion.
D	Damping.
$i,$	Current (p. u.).
$\boldsymbol{k_p}, \boldsymbol{k_i}$	Parameters of the PI controllers.
$\boldsymbol{L_s}, \boldsymbol{L_k}$	Stator/ Leakage inductance (p. u.).
$\boldsymbol{L_m}$	Mutual inductance (p.u.).
$\boldsymbol{r_s}, \boldsymbol{r_r}$	Stator and rotor resistances (p. u.).
$\boldsymbol{T_{ci}}$	Switching small time constant.
u	Voltage (p. u.).
$\boldsymbol{U}$	Independent terms matrix.
$\mathbf{R}, \mathbf{L}$	State model matrixes.
$\mathbf{X}$	Vector of state variables.
$\boldsymbol{\vartheta}$	Normalized state variable integral.
$\boldsymbol{\psi_m}$	Airgap flux linkage (p.u.).
$\boldsymbol{\omega_b}$	Base frequency (rad/s).
$\boldsymbol{\omega_{cross}}$	Crossing frequency (rad/s).
$\boldsymbol{\omega_{band}}$	Bandwidth (rad/s).
$\boldsymbol{\omega_m}$	Rotor speed (p. u.).
$\boldsymbol{\omega_s}, \boldsymbol{\omega_r}$	Speed of the common reference frame, slip frequency.

Superscripts

*	Reference value.

Subscripts

d, q	Variables on rotor moving reference frame.
s, r	Stator/ rotor.
ol, cl	Open loop/ closed loop.

I. INTRODUCTION

The Doubly-fed Induction Generator (DFIG), interfaced with the ac mains, is one of the most popular systems in wind energy conversion systems [1]. For the interconnection of wind generators in wind farms, dc power systems are receiving more interest [2]. In these applications, the dc version of the DFIG, the DFIG-dc, is attractive because it simplifies dc interconnection, [3], [4]. The dual voltage source inverter (VSI) version, Fig. 1, is also a possible choice. In this system a wound rotor induction machine (WRIM) is fed by the stator and rotor by two VSI converters connected to a common dc link. Recently, optimizing efficiency and thus reducing losses has become a major concern in DFIG-dc systems [5] - [9]. A comprehensive minimum-loss control strategy, obtained using Lagrange multipliers, was presented in [9]. This strategy leads to three simple rules for carrying out minimum loss condition. A possible control system, using airgap flux orientation, was also presented in [9]. A first stability study was presented in [10]. In this paper additional insights are introduced. The synthesis of the Proportional Integral (PI) controllers using symmetrical optimum and ITAE (Integral of the time weighted absolute error) criteria are compared. This leads to different PI parameters, dynamics, and stability.

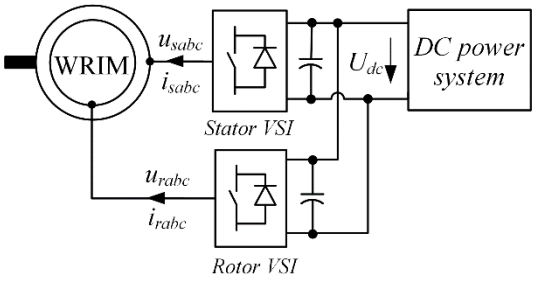

Fig. 1 System Layout.

Section II present the background of the strategy under study, [9]. Section III briefly presents the model of the system in open and closed loop. The synthesis of the PI flux and rotor current controllers, for optimal operating points is presented in section IV. The closed-loop operation is then studied

introducing the dynamics of PI controllers and leading to an 8th-order dynamic model. The stability is analyzed by computing the eigenvalues of the state matrix in Section V. Section VI presents the conclusion.

II. Minimum-Loss Control Strategy

The optimization and control system presented in [9] is based on airgap flux orientation. The theory developed for this method provides three conditions for minimum loss operation.

The first optimal condition allows the optimal stator and rotor frequency to be obtained. In practice, this condition leads to optimal slip values close to ($s = -1$). Fig. 2 presents a phasor diagram of the system in this case.

The second optimal condition gives the optimal d-axis current split between stator and rotor. If VSI losses are neglected, it results $r_s i_{sd} = r_r i_{rd}$.

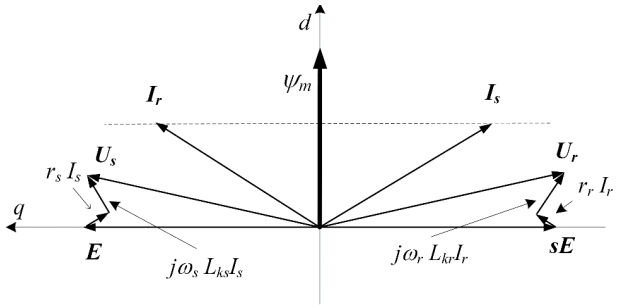

Fig. 2 Steady state phasor diagram for ($s = -1$) close to the minimum loss control point of operation (airgap flux reference frame).

The third optimal condition tells that the optimal flux value makes two suitable ancillary functions P_{d-axis} and P_{q-axis} (defined in [9]) equal to each other. Therefore, the airgap flux should be adjusted by the control system to force these two terms to match.

Fig. 3 presents the optimal airgap flux surface and shows that there are four different operating regions:

A – Minimum flux region: for small torque, when the flux hits the minimum value set at 0.5 p. u..

B – Low torque region: field weakening for reducing core loss – no constraints active; here the optimal flux depends strongly on torque and weakly on speed.

C – Maximum flux region: for high torque and low-medium speeds.

D – Maximum voltage region: voltage constraint active, this is the classic flux weakening region.

The third condition is implemented by adjusting the reference airgap flux controller.

The block diagram of the control implementation method from [9] is presented in Fig. 4. The airgap flux is controlled using two PI controllers whose outputs are the stator voltage components. The q-axis reference flux component is set at zero to synchronize the reference frame with the airgap flux, implementing flux orientation. The flux reference is obtained by a "flux optimizer" block that implements the third optimal condition by forcing the difference "P_{d-axis} - P_{q-axis}" to zero.

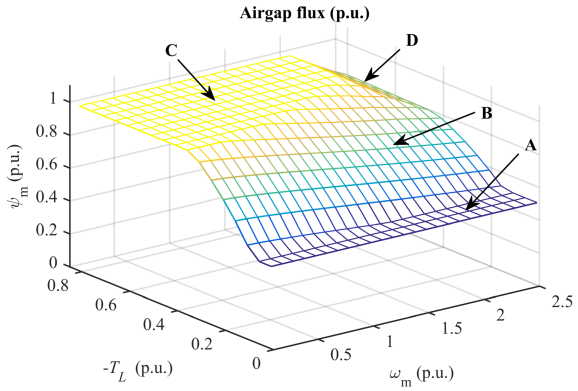

Fig. 3 Airgap flux from numerical optimization, [9].

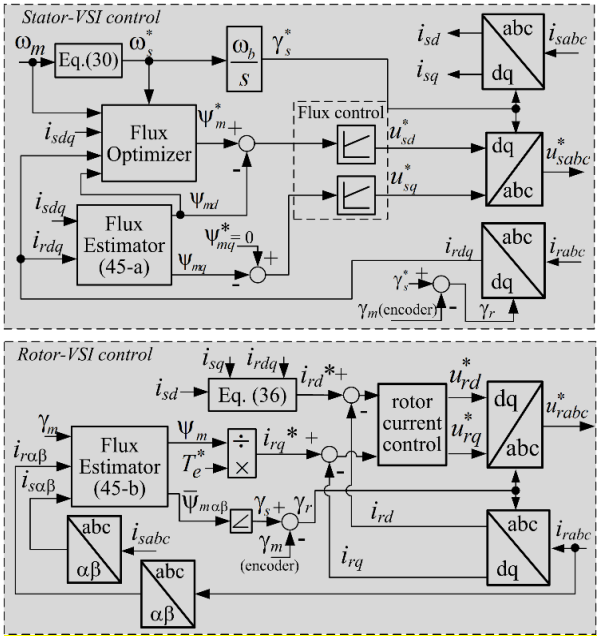

Fig. 4 Control implementation, [9].

Rotor currents are directly controlled using two PI controllers, one setting the d-axis component determined by the optimal split condition, and the other one setting the q-axis current which is related to the torque set-point.

III. Model For Stability Analysis

The input functions of the system analyzed in this paper and represented in Fig. 4 are rotor speed and torque. The strategy optimizes the dual DFIG-DC system for any rotor speed and torque. The rotor connection with the outer system is not considered here. This depends on the application where the system is used.

Because the control system is implemented using airgap flux orientation, the appropriate variables for the study are the d- and q-axis airgap flux and rotor current components. Using these variables in p. u. values, and expressing the time in seconds, results the matrix formalism for the system in open loop [10]:

$$\mathbf{U}_{ol} = \mathbf{R}_{ol}\mathbf{X}_{ol} + \mathbf{L}_{ol}\,\frac{1}{\omega_b}\frac{d\mathbf{X}_{ol}}{dt} \qquad (1)$$

Where the matrices are:

$$\mathbf{U}_{ol} = \begin{bmatrix} u_{sd} \\ u_{sq} \\ u_{rd} \\ u_{rq} \end{bmatrix} \qquad \mathbf{X}_{ol} = \begin{bmatrix} \psi_{md} \\ \psi_{mq} \\ i_{rd} \\ i_{rq} \end{bmatrix} \tag{2}$$

$$\mathbf{R}_{ol} = \begin{bmatrix} \frac{r_s}{L_m} & -\omega_s \frac{L_s}{L_m} & -r_s & \omega_s L_{ks} \\ \omega_s \frac{L_s}{L_m} & \frac{r_s}{L_m} & -\omega_s L_{ks} & -r_s \\ 0 & -\omega_r & r_r & -\omega_r L_{kr} \\ \omega_r & 0 & \omega_r L_{kr} & r_r \end{bmatrix} \tag{3}$$

$$\mathbf{L}_{ol} = \begin{bmatrix} \frac{L_s}{L_m} & 0 & -L_{ks} & 0 \\ 0 & \frac{L_s}{L_m} & 0 & -L_{ks} \\ 1 & 0 & L_{kr} & 0 \\ 0 & 1 & 0 & L_{kr} \end{bmatrix} \tag{4}$$

The first optimality condition returns an optimal slip close to $s = -1$. Thus, for a constant rotor speed, ω_m, it results two symmetrical values $\omega_s = \omega_m/2$ and $\omega_r = -\omega_m/2$. These are algebraic functions that set the two frequencies in function of an input variable ω_m. For constant values of rotor speed ω_m, and consequently of the stator and rotor frequencies, the resulting dynamic system is a linear time-variant system. Thus, it is not necessary to linearize the equations around an operating point. Since the system cannot be used in open loop, this analysis is not reproduced in this paper, [10].

The model in closed loop is presented in [10]. To easy the readiness of this paper, it is briefly described here. The model uses similar variables and parameters when symmetrical optimum method of design of PI controllers or ITAE are used. Only the parameters values are different. The general equation for PI controllers can be written as:

$$y_{out} = k_p(x^* - x) + \omega_b k_i \int (x^* - x) dt \tag{5}$$

Defining the p. u. integral of variable *x* (time in seconds) as:

$$\vartheta = \omega_b \int x \, dt \qquad \text{that is} \qquad x = \frac{1}{\omega_b}\frac{d\vartheta}{dt} \tag{6}$$

4 new state equations and variables should be considered:

$$0 = -\psi_{md} + \frac{1}{\omega_b}\frac{d\vartheta_{md}}{dt} \tag{7}$$

$$0 = -\psi_{mq} + \frac{1}{\omega_b}\frac{d\vartheta_{mq}}{dt} \tag{8}$$

$$0 = -i_{rd} + \frac{1}{\omega_b}\frac{d\vartheta_{rd}}{dt} \tag{9}$$

$$0 = -i_{rq} + \frac{1}{\omega_b}\frac{d\vartheta_{rq}}{dt} \tag{10}$$

Introducing (5) - (10) into the model yields the following 8th-order closed-loop model.

$$\mathbf{U}_{cl} = \mathbf{R}_{cl}\mathbf{X}_{cl} + \mathbf{L}_{cl}\,\frac{1}{\omega_b}\frac{d\mathbf{X}_{cl}}{dt} \tag{11}$$

Where the matrixes are defined as (12), (13) and (14).

$$\mathbf{U}_{cl} = \begin{bmatrix} k_{p\psi}\psi^*_{md} + \omega_b k_{i\psi}\int \psi^*_{md}\, dt \\ k_{p\psi}\psi^*_{mq} + \omega_b k_{i\psi}\int \psi^*_{mq}\, dt \\ k_{pi} i^*_{rd} + \omega_b k_{ii}\int i^*_{rd}\, dt \\ 0 \\ 0 \\ 0 \\ 0 \\ 0 \end{bmatrix} \qquad \mathbf{X}_{cl} = \begin{bmatrix} \psi_{md} \\ \psi_{mq} \\ i_{rd} \\ i_{rq} \\ \vartheta_{md} \\ \vartheta_{mq} \\ \vartheta_{rd} \\ \vartheta_{rq} \end{bmatrix} \tag{12}$$

$$\mathbf{R}_{cl} = \begin{bmatrix} \frac{r_s}{L_m} + k_{p\psi} & -\omega_s\frac{L_s}{L_m} & -r_s & \omega_s L_{ks} & k_{i\psi} & 0 & 0 & 0 \\ \omega_s\frac{L_s}{L_m} & \frac{r_s}{L_m} + k_{p\psi} & -\omega_s L_{ks} & -r_s & 0 & k_{i\psi} & 0 & 0 \\ \frac{-\frac{k_{pi}}{L_m}}{\left(1+\frac{r_r}{r_s}\right)} & -\omega_r & r_r + k_{pi} & -\omega_r L_{kr} & \frac{-\frac{k_{ii}}{L_m}}{\left(1+\frac{r_r}{r_s}\right)} & 0 & k_{ii} & 0 \\ \omega_r & 0 & \omega_r L_{kr} & r_r + k_{pi} & 0 & 0 & 0 & k_{ii} \\ -1 & 0 & 0 & 0 & 0 & 0 & 0 & 0 \\ 0 & -1 & 0 & 0 & 0 & 0 & 0 & 0 \\ 0 & 0 & -1 & 0 & 0 & 0 & 0 & 0 \\ 0 & 0 & 0 & -1 & 0 & 0 & 0 & 0 \end{bmatrix} \tag{13}$$

$$\mathbf{L}_{cl} = \begin{bmatrix} \frac{L_s}{L_m} & 0 & -L_{ks} & 0 & 0 & 0 & 0 & 0 \\ 0 & \frac{L_s}{L_m} & 0 & -L_{ks} & 0 & 0 & 0 & 0 \\ 1 & 0 & L_{kr} & 0 & 0 & 0 & 0 & 0 \\ 0 & 1 & 0 & L_{kr} & 0 & 0 & 0 & 0 \\ 0 & 0 & 0 & 0 & 1 & 0 & 0 & 0 \\ 0 & 0 & 0 & 0 & 0 & 1 & 0 & 0 \\ 0 & 0 & 0 & 0 & 0 & 0 & 1 & 0 \\ 0 & 0 & 0 & 0 & 0 & 0 & 0 & 1 \end{bmatrix} \tag{14}$$

The model should include the condition of optimal d-axis current split. Using an estimate of ψ_{md} the rotor d-axis reference current is computed.

$$i^*_{rd} = \frac{1}{\left(1+\frac{r_r}{r_s}\right)L_m}\psi_{md} \tag{15}$$

This is introduced in the model by suppressing the 3rd element in $\mathbf{U}_{cl}$ matrix and changing elements "(3,1)" and "(3,5)".

This model ignores the delay related to the switching process of the semiconductors represented by a small time-constant T_{ci}. It can be introduced in the model easily, then resulting in a 12th-order model. Only the poles that are far from the origin differ from those of the 8th-order model.

The stability analysis in closed loop can now be performed computing the system matrix $\mathbf{A} = \mathbf{L}_{cl}^{-1}\,\mathbf{R}_{cl}$ and its eigenvalues.

The system in closed loop is characterized by eight almost all complex-conjugate poles.

IV. Synthesis of the PI Controllers

A. Using symmetrical optimum criterium

The synthesis of the PI controllers using symmetrical optimum criterium can be found in [11]. This uses a design parameter a, related to damping of the oscillatory portion of the response $D = (a-1)/2$. Formulas for PI parameter calculation based on this criterium are presented in [10]. Here, only the final formulas are shown. Note that, when p. u. variables are used, the true integral parameter in (5) is $\omega_b k_i$.

1) Airgap Flux Controller

The flux PI controller gains are as follows [10]:

$$k_{p\psi} = \frac{1}{a}\frac{1}{\omega_b T_{ci}}\frac{L_s}{L_m} = \frac{\omega_{cross}}{\omega_b}\frac{L_s}{L_m} \tag{16}$$

$$k_{i\psi} = \frac{1}{a^3 T_{ci}^2}\frac{1}{\omega_b^2}\frac{L_s}{L_m} = \frac{\omega_{cross}^2}{a\,\omega_b^2}\frac{L_s}{L_m} \tag{17}$$

The open-loop cross-over frequency is given by:

$$\omega_{cross} = \frac{1}{aT_{ci}} \tag{18}$$

2) Rotor current control

Since the equations are similar, it results:

$$k_{pi_r} = \frac{\omega_{cross}}{\omega_b} L_{kr} \qquad k_{ii_r} = \frac{\omega_{cross}^2}{a\,\omega_b^2} L_{kr} \tag{19}$$

B. Using ITAE criterion

1) Air-gap flux control

The open-loop transfer function can be written as:

$$G_{eq} = \frac{k_p s + \omega_b k_i}{s}\frac{L_m}{r_s + L_s\frac{s}{\omega_b}} \tag{20}$$

The ITAE criterion uses the PI zero cancelling the pole,

$$\frac{k_p}{\omega_b k_i} = \frac{L_s}{r_s \omega_b} \tag{21}$$

Replacing in the transfer function, in closed loop, results:

$$\frac{G_{eq}}{1+G_{eq}} = \frac{1}{1+s\frac{r_s}{\omega_b k_i L_m}} \tag{22}$$

In terms of closed loop bandwidth, ω_{band}, the PI parameters for flux control become:

$$k_{p\psi} = \frac{L_s}{L_m}\frac{\omega_{band}}{\omega_b} \qquad k_{i\psi} = \frac{r_s}{L_m}\frac{\omega_{band}}{\omega_b} \tag{23}$$

2) Rotor current control

Considering only the main loop, and neglecting the disturbance terms, the rotor current control can be modelled as:

$$G_{eq} = \frac{k_p s + \omega_b k_i}{s}\frac{1}{r_s + L_{kr}\frac{s}{\omega_b}} \tag{24}$$

As this is like the airgap flux controller, results for the rotor current controller:

$$k_{pi_r} = \frac{\omega_{band}}{\omega_b} L_{kr} \qquad k_{ii_r} = \frac{\omega_{band}}{\omega_b} r_r \tag{25}$$

In this paper PI controllers are synthesized to have higher closed loop bandwidth for rotor current control than for airgap field control. This second control loop is used, in a slow process, to adjust the flux level to have minimum losses. The switching frequency was assumed to be 2 kHz. For airgap field control a bandwidth close to 2 p. u. was assumed. In the case of the symmetrical optimum criterium this corresponds approximately to a=8. For rotor current control it was used a=3. This leads to 6 p. u. bandwidth that is usual in industry. The parameters using ITAE were obtained directly using (23) and (25). They are presented in Table 1.

TABLE I. PI Parameters

	Air-gap flux controller		Rotor current controller	
	$k_{p\psi}$	$k_{i\psi}$	k_{pir}	k_{iir}
ITAE	2.13	0.08	0.6	0.3
Symmetrical optimum	1.7	0.34	0.42	0.6

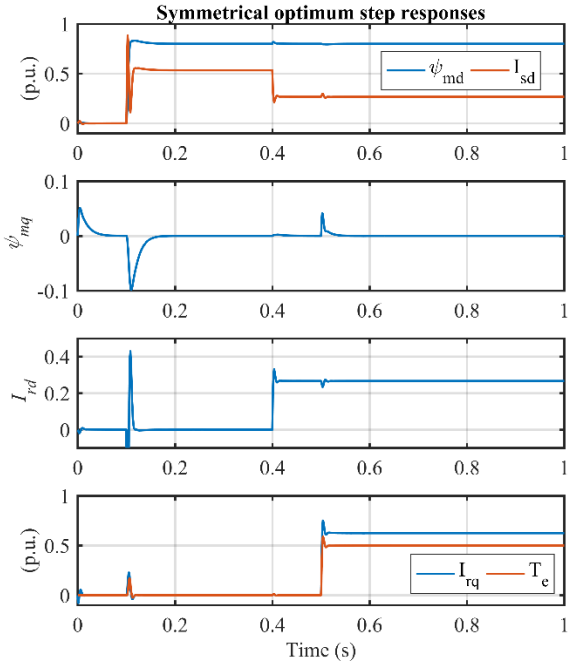

Fig. 5 Response to steps using symmetrical optimum criterion.

Fig. 5 presents simulation results to steps on the reference flux (at $t = 0.1\ s$), followed by a step on the reference rotor d-

axis current at ($t = 0.4\ s$) followed by a step on the rotor q-axis reference at ($t = 0.5\ s$).

From Fig. 5, it can be concluded that the flux is controlled accurately with some minor influence of disturbances in the q-axis flux controller, that is, the flux orientation is kept operating when perturbations occur. The rotor current controllers preform also well.

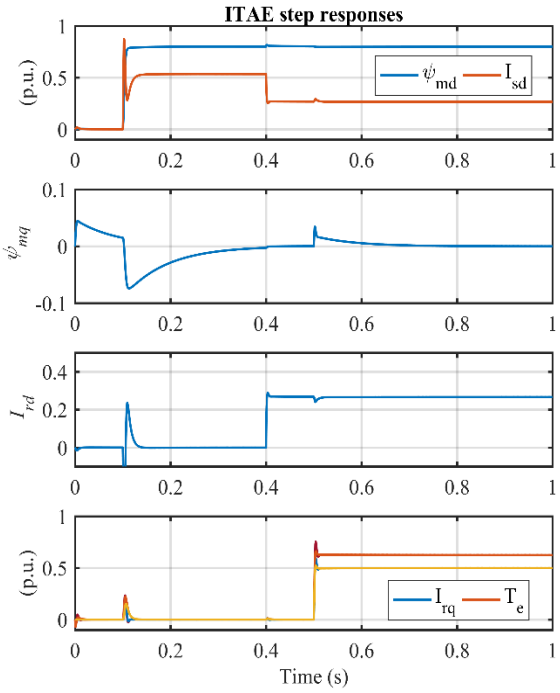

Fig. 6 Step response using ITAE criterion.

For the PI controllers synthesized using the ITAE criterium, similar results, Fig. 6, were obtained. The q-axis flux response is not as good as in the previous case. The system become more sensitive to external disturbances. Since the closed loop bandwidth is similar, the resulting responses to steps in the references becomes also similar.

V. Stability Analysis Results

A. *Stability study using PI parameters properly synhesized*

1) Symmetrical optimum

Fig. 7 presents all the closed-loop eigenvalues when the rotor speed varies within the 0.01 - 2 p. u. range. The pole variation in the complex plane is due to the influence of the terms neglected in the PI synthesis. Fig. 7 shows that the damping worsens at high rotor speed, but remains acceptable for the usual speed range [0 - 2 p. u.]. Fig. 8 shows only the dominant poles. The system has a good damping characteristic. It behaves as a second order system and, for dominant poles, the negative real part is always greater than the imaginary part.

If a 12th-order model were used considering the power electronics semiconductors switching delay, there would be no significantly different results.

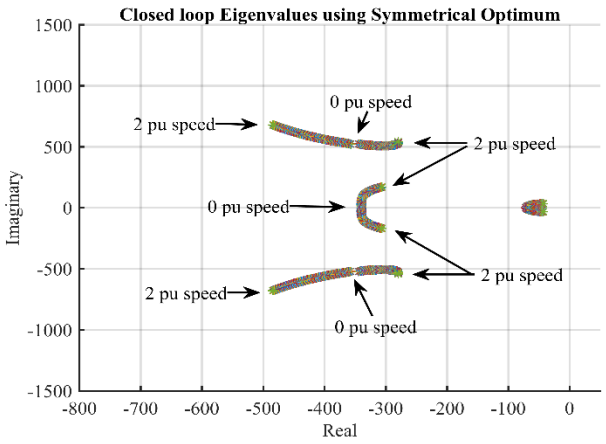

Fig. 7 All closed loop eigenvalues using the symmetrical optimum.

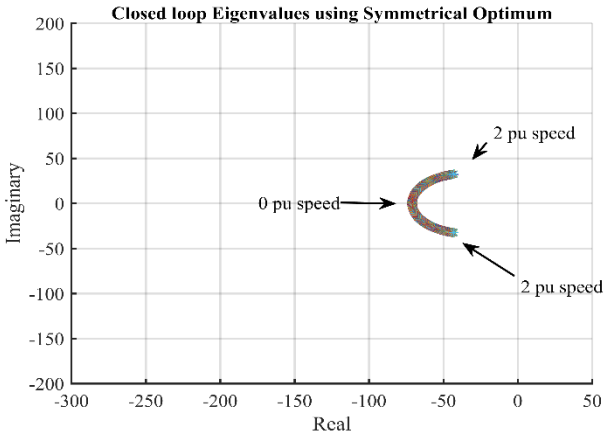

Fig. 8 Dominant closed loop eigenvalues using the symmetrical optimum.

2) ITAE

As in the previous case, the system has also 8 poles that moves on the plane. The dominant poles are shown in Fig. 9.

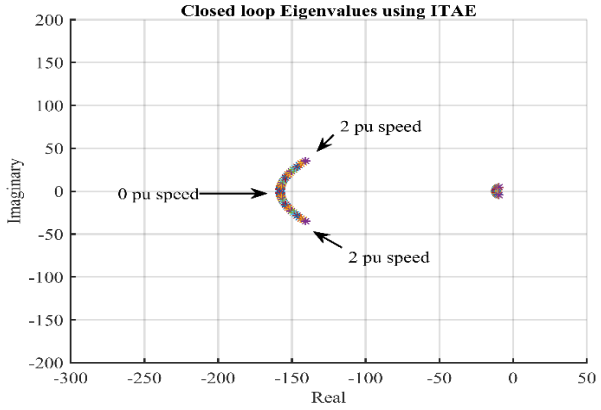

Fig. 9 Dominant closed loop eigenvalues using the ITAE criterium.

In this case the most dominant poles are closer to the origin. If a higher flux controller bandwidth is used, for example 4 p.u., no significant modification on the dominant poles is found. For lower bandwidths considered in the design (in a reasonable range) the stability is guaranteed if the criteria (16), (17), (19) or

(23, (25) rules are respected. The poles move in the complex plane but remain in the stability zone.

B. Instability under de-tuned PI parameters

Instability can occur when the PI parameters differ from the ones computed in section IV. For example, the poles obtained when $k_{p\psi} = 0$ are presented in Fig. 10 and Fig. 11, showing instability. At zero speed, in the symmetrical optimum case, the poles are on the complex positive real half plane. When speed increases, these two pairs follow different trajectories. For the ITAE case, at zero speed, both poles are in the stability zone but with increasing speed two poles cross the stability border and return to stability again.

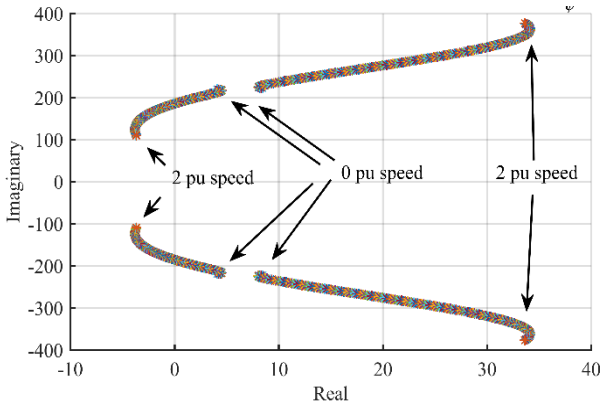

Fig. 10 Instability using the symmetrical optimum. ($k_{p\psi} = 0$).

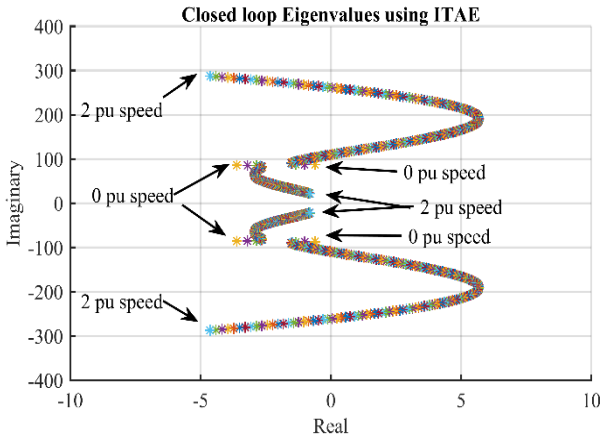

Fig. 12 Instability using the ITAE criterium. ($k_{p\psi} = 0$).

VI. Conclusion

Some aspects of the stability of the dual-VSI DFIG minimum-loss control strategy are presented in this paper.

The symmetrical optimum criterion, as well as the ITAE criterium for designing PI controllers are presented and used for control and stability analysis. This was made computing the eigenvalues of the system model in closed loop. It is shown that under normal conditions the system is stable independently of the rotor speed and load level. However, when the PI parameters are far from the optimal ones, for example when $k_{p\psi} = 0$, instability can occur.

Appendix

Wound Rotor Induction Machine ratings: 3.2 kW, 4-pole, 380/110 V, 8.1/19 A. Per-unit parameters: r_s=0.06, r_r =0.05, L_m=1.5, L_{ks}=0.10, L_{kr}=0.10. Base values: S_B=5350 VA, f_B=50 Hz, U_B= 380 V, T_B=34 Nm.

Acknowledgment

This work was supported by FCT, "Fundação para a Ciência e Tecnologia" under project UIDB/50021/2020. It is also funded by FCT/MCTES through national funds and when applicable co-funded by EU funds under the project UIDB/EEA/50008/2020.

References

[1] R. Cárdenas, R. Peña, S. Alepuz, G. Asher, "Overview of control systems for the operation of DFIGs in wind energy applications," *IEEE Trans. Ind. Electron*., vol. 60, no. 7, pp. 2776–2798, July 2013.

[2] S. Yan, A. Zhang, H. Zhang and J. Wang, "Control scheme for DFIG converter system based on DC-transmission," in *IET Electric Power Applications*, vol. 11, no. 8, pp. 1441-1448, 9 2017.

[3] G. D. Marques, M. F. Iacchetti, "DFIG topologies for DC networks: a review on control and design features," *IEEE Trans. Pow. Electron*., vol. 34, no. 2, pp. 1299-1316, Feb. 2019.

[4] H. Nian, X. Yi, "Coordinated control strategy for doubly-fed induction generator with dc connection topology," *IET Renew. Power Gener*., vol. 9, no. 7, pp. 747–756, Aug. 2015.

[5] Y. Han and J. I. Ha, "Control Method of Double Inverter Fed Wound Machine for Minimizing Copper Loss in Maximized Operating Area," *IEEE Trans. on Ind. Electron*., vol. 64, no. 10, pp. 7700-7710, Oct. 2017.

[6] B. Zhang, W. Hu, and Z. Chen, "Loss minimizing operation of doubly fed induction generator based wind generation systems considering reactive power provision," in Proc. 40th Annu. Conf. IEEE Ind. Electron. Soc., 2014, pp. 2146–2152.

[7] G. D. Marques, M. F. Iacchetti, "Field Weakening Control for Efficiency Optimization in a DFIG connected to a dc Link" *IEEE Trans. Ind. Electron*., Vol. 63, No.6, pp. 3409 – 3419, June. 2016.

[8] S. M. A. Cruz, G. D. Marques, P. F. C. Gonçalves and M. F. Iacchetti, "Predictive Torque and Rotor Flux Control of a DFIG-DC System for Torque Ripple Compensation and Loss Minimization," *IEEE Trans. on Ind. Electron*, vol. 65, no. 12, pp. 9301-9310, Dec. 2018.

[9] G. D. Marques, Sérgio M. A. Cruz, Matteo F. Iacchetti, "Minimum-Loss Control Strategy for a Dual-VSI DFIG DC System" *IEEE Trans on Ind. Electron*., Vol. 67, no. 10, pp. 8175-8185, Oct. 2019.

[10] G. D. Marques, Matteo F. Iacchetti, Sérgio M. A. Cruz, "Stability Study of a Minimum-Loss Control Strategy for a Dual-VSI DFIG DC System" 2020 IEEE 14th International Conference on Compatibility, Power Electronics and Power Engineering (CPE-POWERENG) pp. 297-302, 2020.

[11] Werner Leonard, "Control of Electrical Drives" SpringerVerlag, 1984, p.72-74.